IEICE TRANS. INF. & SYST., VOL.E103–D, NO.11 NOVEMBER 2020

PAPER

Design and Performance Analysis of a Skin-Stretcher Device for Urging Head Rotation

Takahide ITO[†a)], ***Nonmember***, **Yuichi NAKAMURA**[††b)], **Kazuaki KONDO**[††c)], ***Members***, **Espen KNOOP**[†††d)], ***and*** **Jonathan ROSSITER**[†††e)], ***Nonmembers***

SUMMARY This paper introduces a novel skin-stretcher device for gently urging head rotation. The device pulls and/or pushes the skin on the user's neck by using servo motors. The user is induced to rotate his/her head based on the sensation caused by the local stretching of skin. This mechanism informs the user when and how much the head rotation is requested; however it does not force head rotation, i.e., it allows the user to ignore the stimuli and to maintain voluntary movements. We implemented a prototype device and analyzed the performance of the skin stretcher as a human-in-the-loop system. Experimental results define its fundamental characteristics, such as input-output gain, settling time, and other dynamic behaviors. Features are analyzed, for example, input-output gain is stable within the same installation condition, but various between users.

key words: *user interface, motion induction, skin stretcher, head rotation, human-in-the-loop system, motion analysis*

1. Introduction

With the recent advances of communication technologies, a variety of devices for haptic and force information transmission have been developed and become available. Those devices enable us to feel touch, force, and movement at a remote place. Such advanced technology also provides us empathic communication, e.g., awareness of remote people and feelings of working or living with them, etc. We can consider a variety of potential applications. Informing and prompting good motions provides intuitive supports for sports, job training, and rehabilitation [1]. Communicating touch or movement information provides good tools for remote care, nursery, and intimate communication for family members [2]. Sharing motion information can support group activities that require mutual awareness, or joint force at coordinated timing. As an effective means of this type of communication, we focused on skin sensations, especially the sensation of skin stretching.

We designed a novel device that induces head rotation by locating stretching the skin.This mechanism provides feasible functions for the above purposes. In the following sections, we will introduce the idea of the skin-stretcher device, its function, and its performance measured through our experiments.

2. Related Work

A variety of methods for force application or power assist have been proposed that work intuitively and immediately. Electric muscle stimulating (EMS) or galvanic vestibular stimulation (GVS) has been also considered. Aoyama et al. showed that GVS can be used for triggering head movements and body sway [4]. Contrastly, we focus on assistance that applies touch sensations through the application of weak forces. There are many situations in which gentle assistance is necessary, since inappropriate application of strong force can be dangerous, e.g., applying unexpected force to a person can lead him/her to lose balance.

Methods without enforcing movements have also been widely proposed. Typically, senses of vision and audio are used for teaching or inducing motion. Maeda et al. proposed machine manipulation assistance by providing the first-person's view of an expert [5]. Asakura et al. proposed a method for guiding motion by using sound generated from electromyography (EMG) [6]. However, a user's vision and hearing senses may be fully occupied with a task, implying that we must find other modalities for safe human interaction when the user is occupied in performing a task.

Another way of inducing the user's motions is artificial control of their sense of equilibrium. Motions are modified while the user intuitively moves based on their controlled feeling. Kon et al. made a hanger reflex device that evokes head rotation [7], and proved that walking direction can be modified by the device. Amemiya et al. have proposed a method to induce directional force perception using a lopsided vibrator devic [8]. Those works proved that our motions can be affected by well-designed devices.

Based on these considerations, we chose skin sensation as a supplementary means for transmitting motion information or inducing motions. Preceding studies have proved the potential of skin sensation in transmitting small displacements, direction, and tickling. Ion et al. designed a device that stretches the arm's skin in various directions and mea-

Manuscript received June 28, 2019.
Manuscript revised May 25, 2020.
Manuscript publicized August 3, 2020.

[†]The author is with Graduate School of Engineering, Kyoto University, Kyoto-shi, 606–8501 Japan.
[††]The authors are with Academic Center for Computing and Media Studies, Kyoto University, Kyoto-shi, 606–8501 Japan.
[†††]The authors are with University of Bristol & Bristol Robotics Laboratory Department of Engineering Mathematics, University of Bristol Merchant Venturers Building, Woodland Road, Bristol BS8 1UB, UK.
a) E-mail: itou@ccm.media.kyoto-u.ac.jp
b) E-mail: yuichi@media.kyoto-u.ac.jp
c) E-mail: kondo@ccm.media.kyoto-u.ac.jp
d) E-mail: espen.knoop@disneyresearch.com
e) E-mail: Jonathan.Rossiter@bristol.ac.uk
DOI: 10.1587/transinf.2019EDP7184

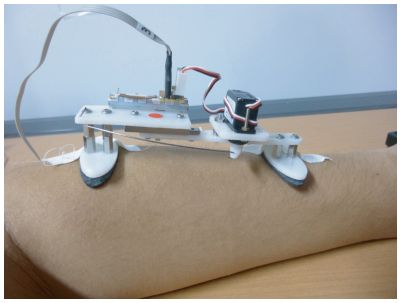

Fig. 1 Skin-stretcher device designed at University of Bristol [3]

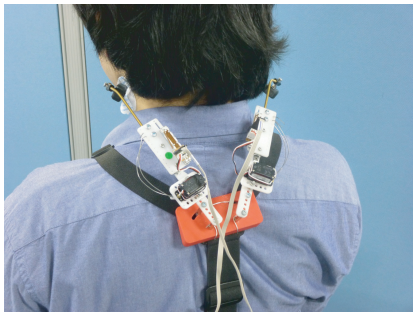

Fig. 2 The skin-stretcher device attached to the neck

sured the accuracy of the participants' perceived displacement [9]. They proved that various shapes can be indicated by using skin sensation. Mizukami et al. designed a tactile presentation device by a shape-memory alloy, and proved that apparent movements and rubbing sensations can be successfully presented [10]. Knoop et al. designed a device, which strokes the skin and delivers various sensations, including tickling sensation [11]. Levesque et al. investigated a display for Braille dots by lateral deformation, and showed its performance and changing sensitivity depending on the amplitude and duration of the stroking [12].

In contrast, our focus is on inducing motions by skin sensation. A preceding research work for this purpose is the skin stretcher as shown in Fig. 1, which was introduced by Rossiter et al. [3]. The device pushes/pulls the skin by contracting or expanding itself through a link structure driven by a servo motor. It is designed to induce a motion that is consistent with the sensation of skin stretch. Although the device has potential for tactile communication, its performance has not been fully explored.

3. System Design

3.1 Mechanism of Device

Figure 2 and 3 show our skin-stretcher device and its mechanism, respectively. The skin-stretcher consists of two main components; one part changes length by the rotation of the servo motor, and the other measures its approximate length with a linear potentiometer. Additionally, two sticky pads with ball joints and a body-mount harness are equipped for fixing the device to the head and the body. This design enables adjustment of the device to the user's body size, and the device can gently and locally push or pull the skin. Note that the spring installed between the motor and the slider works as a buffer for movement inconsistency between the head and the device to some extent. A similar function is also provided by the elasticity of the skin.

The primary features of the device are listed below.

- Skin stretch provides natural and intuitive stimulus that directly but subtly indicates the direction of head rotation.
- The device does not apply strong force that compels the user to move against the user's intention. The user can override the stimulus and prioritize voluntary movements if necessary.
- The device can be used not only for inducing motions but also for informing the feeling of motions. The user can feel the movement of the pads even if the user does not move as requested by the device.

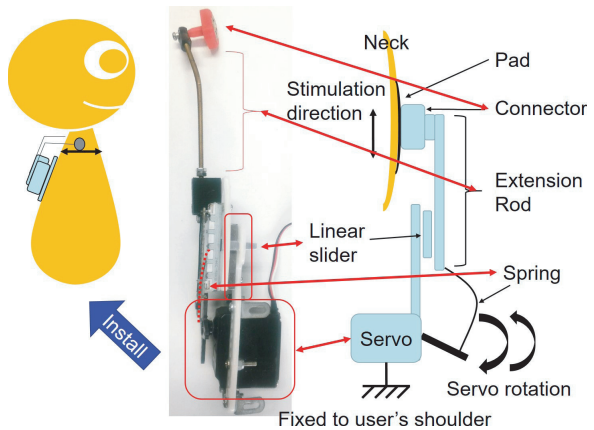

Fig. 3 Mechanism of the skin-stretcher device

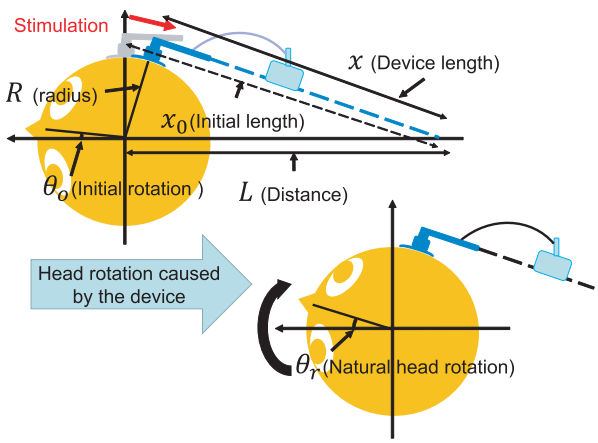

Fig. 4 Geometry and action of the device

3.2 Input and Output Model

Figure 4 shows the geometry of the device and the head.

The device is initially attached with the condition that the extension rod is parallel to the tangent of the neck. We approximate the relation between the natural head rotation and the device length by the following formulas:

$$R^2 + x_0^2 = L^2 \tag{1}$$

$$\cos\left(\frac{\pi}{2} - \theta_r\right) = -\frac{R^2 + L^2 - x^2}{2RL} \tag{2}$$

where R is the approximated radius of the neck, L is the distance between the center of the device and the center of the neck, x and x_0 are the actual and the initial length of the skin-stretcher device, respectively. θ_r is the natural head rotation at which the user feels no skin stretch. It is represented by the angle between the orientation from the center of the neck toward the pad and the vertical axis as shown in Fig. 4. θ_o is the initial head rotation.

As we consider the above mechanism as a man-machine system, the virtual input to the system is the head rotation angle $\Delta\theta_r$ requested by the skin displacement, which is caused by $\theta_r - \theta_o$. We do not directly use the rotation angle of the servo motor for calculating the input value because the extension rod and the servo motor are connected by the elastic link, i.e., the rotation angle of the servo motor and the displacement of the rod do not hold stable relationships. Alternatively, the displacement Δx is directly measured by the potentiometer installed in the device. Thus the natural head rotation angle $\Delta\theta_r$ can be estimated using Δx by the above equations.

The output (response) of the system is the actual head rotation angle $\Delta\theta$. This device has no mechanism for measuring the actual head orientation because such a mechanism would make the device more complicated and heavier. In performance analyses, we measured head orientation with a magnetic position sensor (LIBERTY^{TM}). We attached two receiver probes to the front and the back side of the head, respectively. Orientation change of the line connecting two probes represents the head rotation angle.

4. Method for Performance Measuring

4.1 Conditions of Measurements

We gathered data from five male participants between 22 and 26 years old, who did not have any health problems that would affect the experiments. All participants joined the experiments by their own will, and we announced that they could cancel or stop experiments in any stage. The data were handled under the Kyoto University's privacy policy and the Act on the Protection of Personal Information.

The participants were asked to rotate their heads to minimize the feeling of displacement or the tension on the skin caused by the skin-stretcher. To eliminate other stimuli that possibly affect the head rotation, we asked the participants to close their eyes and wear earphones. They block visual clues on how much they rotate their heads and sound clues on when the servo motor operates. Data were collected under varying conditions; trials with inputs with varying angles for each participant.

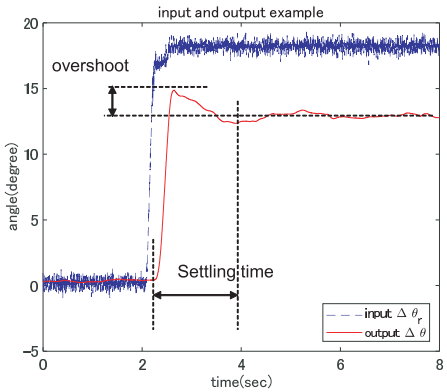

Fig. 5 Example of input and output, Blue line shows angle skin stimulus from skin stretcher device and Red line shows the head angle of the user in response.

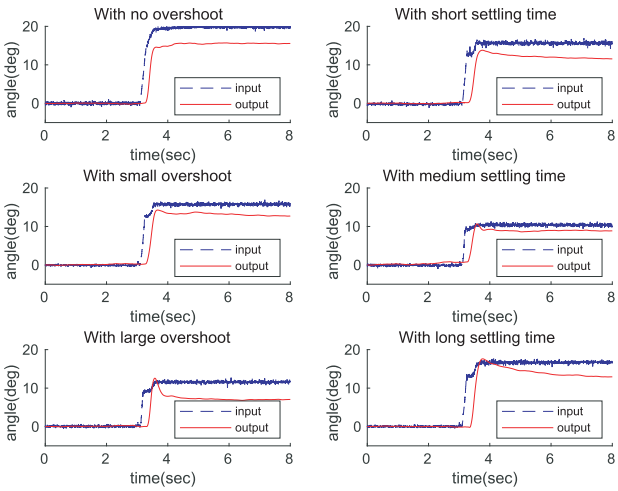

Fig. 6 Examples of outputs (head rotation angle) exhibiting a range of gain, settling times, and overshoot by participant A. Each subfigure shows a response to one of the following rotation angles, 10°, 15° or 20°.

4.2 Characteristics of Data

Figure 5 shows an example of the typical relationship between input $\Delta\theta_r$ (blue line) and output $\Delta\theta$ (red line). We applied a step input to the servo motor. The rotation angle $\Delta\theta_r$ of the servo shows a finite gradient because of the finite speed of the motor and the series elastic element.

Figure 6 shows several examples from the same participant. We can see that gain, settling time, and overshoot vary with amplitude and between tests. Such variation and stability of response and individual difference were examined in the experiments.

5. Performance Analysis

5.1 Gain, Settling Time, and Overshoot

As important characteristics of the output behaviors, we

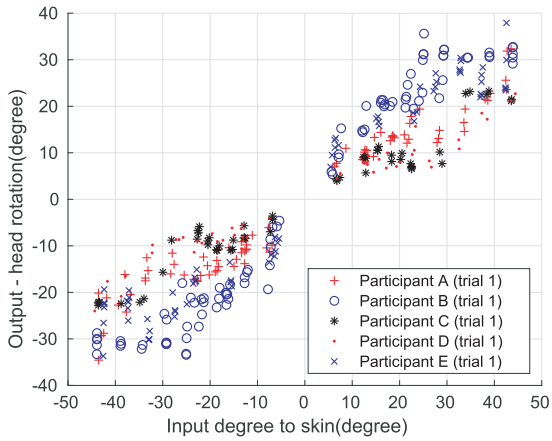

Fig. 7 Input and output for of contiguous sets of trials for the all participants without detaching and re-installing the device. The horizontal axis represents the requested rotation angle ($\Delta\theta_r$), and the vertical axis represents the actual rotation angle ($\Delta\theta$). Each mark represents a single trial.

consider gain, overshoot, and settling time. Gain is the ratio between the input and output after the output was converged. Overshoot is the difference between the peak and the convergence value, and the settling time is the time from the beginning of the input to the time when the output is settled within ±10% of the convergence value.

Figure 7 is a scatter plot of input and output, i.e., ($\Delta\theta_r$, $\Delta\theta$) after the output was converged. Each mark in the figure (circle and triangle) indicates a trial, and a set of marks with the same shape represents a set of contiguous trials by the same participant without detaching and re-installing the device. Each trial contains 4 or 5 head rotations for each $\Delta\theta_r$. These contiguous trials contain different inputs that their angles vary from 5° to 45° with every 5° and that turns to the right or left.

From the graph, proportionality between the requested angle and output is observed, which suggests that gain is relatively stable over trials for each participant with the same device attachment condition. However, we can see different gradients for different participants. Their difference is affected by device attaching conditions, especially the position and the contact of the pad to the skin. Moreover, the linearity of the proportionality was observed to be different among participants.

Based on the above observations, we performed linear regression on the input-output data. Table 1 shows the overview of the result. Table 1 also shows that the calibration after the installation of the device gives a good estimation of the gain with R^2 value of the linear regression around 0.95. The gain remains stable once the device is installed until the device is detached. However, the representative gain ranged from 0.49 to 1.08, which shows significant differences among participants. Table 2 also shows the performance changes that possibly caused by detaching and re-installing the device even for the same participant. The row of participant A was measured when re-installing the device after two-hour interval, and the row of participant B

Table 1 Gain (mean and variance), decision coefficient, and number of head rotations

participant	gain		decision coefficient		number of head rotations
	mean	var	R^2	norm of residuals	
A	0.73	$4.82 * 10^{-2}$	0.95	32.7	81
B	1.08	$8.59 * 10^{-2}$	0.95	54.6	88
C	0.53	$2.21 * 10^{-2}$	0.95	22.1	56
D	0.49	$1.76 * 10^{-2}$	0.95	17.1	57
E	0.95	0.16	0.94	46.3	73

Table 2 Gain (mean and variance), decision coefficient, and number of head rotations after re-installing the device

participant (additional set of trials)	gain		decision coefficient		number of head rotations
	mean	var	R^2	norm of residuals	
A	0.61	$1.90 * 10^{-2}$	0.96	24.2	58
B	0.19	$3.22 * 10^{-3}$	0.94	7.13	88

Table 3 Settling time, Overshoot, and Peak time for all participant

settling time (msec)	mean	432
	standard deviation	169
overshoot (degree)	mean	2.35
	standard deviation	2.23
peak time (msec)	mean	354
	standard deviation	71.5

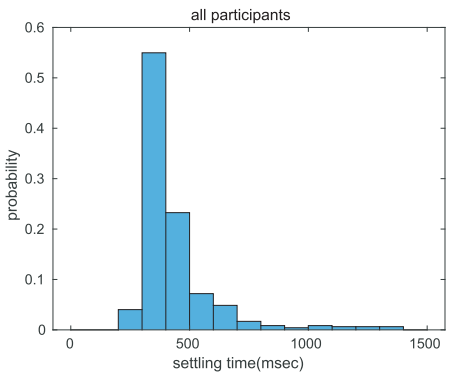

Fig. 8 Histogram of settling time for all participants

was on a different day. These suggest that we can estimate the gain value if a calibration is conducted each time the device is attached, for which we need to estimate the gain by a small number of trials.

Figures 8 and 9 show the histogram of the settling time and overshoot for all participants. Table 3 shows those mean values and standard deviations. Both settling time and overshoot show a range of values depending on device installation and personal difference. Settling time has unimodal distribution, and it shows that head rotation settles in less than 0.6 sec for 89.9% of cases. For overshoot, smaller values are dominant. Both are closely related to dynamic properties of the system, which will be discussed below.

Figure 10 shows the histogram of the peak time, i.e., the timing when the head rotation angle reaches the maximum of the overshoot. The result suggests that we can ap-

Table 4 Examples of parameters for Eq. (3)

Sample ID	a	b	c	d	e	f	fitting rate(%)
1	0.0254	0.483	0.668	$7.26 * 10^{-4}$	0.622	0.622	94.7
2	0.0441	1.38	0.875	$1.97 * 10-3$	0.113	1.64	91.9
3	1.02	2.69	0.769	$9.99 * 10^{-3}$	0.999	3.29	95.9

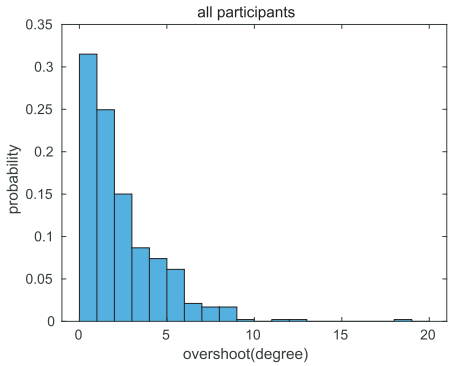

Fig. 9 Histogram of overshoots for all participants

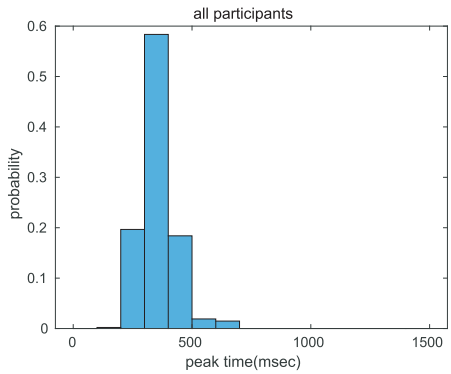

Fig. 10 Histogram of peak time for all participants

proximate the peak time roughly.

5.2 Dynamic Characteristics

For more general characteristics of the system, we examined the transfer function which can be used to estimate dynamic behaviors of head rotation. We consider a simple model where head rotation is caused by the interaction of agonist muscles that rotates the head and antagonist muscles that stops rotation. For this mechanism, we assume a system model below.

$$H(s) = e^{-s\tau}\frac{as^2 + bs + c}{ds^3 + es^2 + fs + 1} \tag{3}$$

This model is based on the following consideration. First, for a motion caused by each muscle, we assume a model with simple first-order lag with dead time, i.e., $e^{-s\tau}\frac{G}{1+Ts}$, where G is gain, T is time constant, and τ is dead time. This modeling is based on preceding studies that have reported that muscle contractions can be roughly approximated by first-order lag with dead time [13]–[15].

Next, assuming that agonist and antagonist have different gains, time constants, and dead times, we obtain the system model as the following.

$$H(s) = e^{-s\tau_1}\frac{G_1}{1+T_1 s} - e^{-s\tau_2}\frac{G_2}{1+T_2 s} \tag{4}$$

Next, we ignore the feedback loop because skin sensation becomes imperceptible as the amount of stretch becomes small. Consequently, we obtain Eq. (5) by denoting $\tau_3 = \tau_2 - \tau_1$ ($\tau_3 > 0$), and apply the first-order Pade estimation that results in $e^{-s\tau_3} \approx \left(1 - \frac{\tau_3 s}{2}\right)/\left(1 + \frac{\tau_3 s}{2}\right)$.

$$\begin{aligned} H(s) &= e^{-s\tau_1}\frac{G_1}{1+T_1 s} - e^{-s\tau_1}\left(\frac{1-\frac{\tau_3 s}{2}}{1+\frac{\tau_3 s}{2}}\right)\frac{G_2}{1+T_2 s} \\ &= e^{-s\tau_1}\left\{\left(G_1 T_2 + G_2 T_1\right)\tau_3 s^2\right. \\ &+ \left(G_1\tau_3 + G_2\tau_3 + 2G_1 T_2 - 2G_2 T_1\right)s \\ &\left.+2G_1 - 2G_2\right\}/\left\{T_1 T_2 \tau_3 s^3\right. \\ &+ \left(2T_1 T_2 + T_1\tau_3 + T_2\tau_3\right)s^2 \\ &\left.+ \left(2T_1 + 2T_2 + \tau_3\right)s + 2\right\} \end{aligned} \tag{5}$$

Thus, we obtain a transfer function as Eq. (3) with a second-order numerator and a third-order denominator.

5.3 System Identification

We verified the consistency between the above system model and the experimental data by system identification. For system identification, we used MATLAB function "tfest" explained in Appendix A and the system model as Eq. (3). Before applying system identification, the dead time for each trial was approximated by the duration between the time when the input exceeds 10% of its maximum and the time when the output exceeds the 10% of its maximum. The result of the system identification for each trial showed 94.7% for the average fitting rate, and 3.42% for the standard deviation. Some of the estimated parameters are shown in Table 4. Examples of better, average, and poor fitting rate are shown in Fig. 11. The simulated results show good fit except for small fluctuations.

Next, we examined the possibility of generating a "personal model" that can represent behaviors of each participant. For this purpose, we took the average of the values obtained for each parameter through all trials of each participant. Gain adjustment is necessary because we cannot directly compare parameters with different gain values caused by different attachment conditions of the device; parameters in the numerator are divided by c in Eq. (3). The mean and standard deviation of parameters are shown in the Table 5. Through all participants, the average fitting rate by

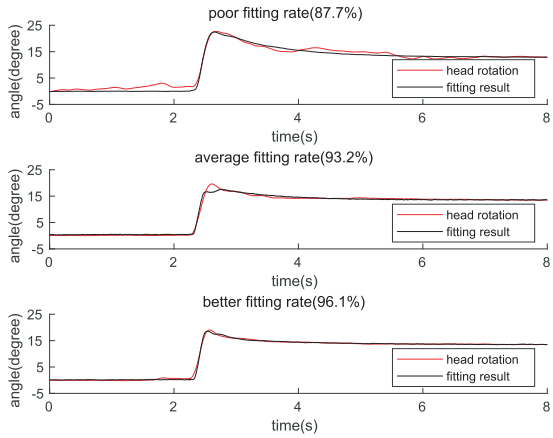

Fig. 11 Simulation with poor (87.7%), average (93.2%), and better (96.1%) fitting rate

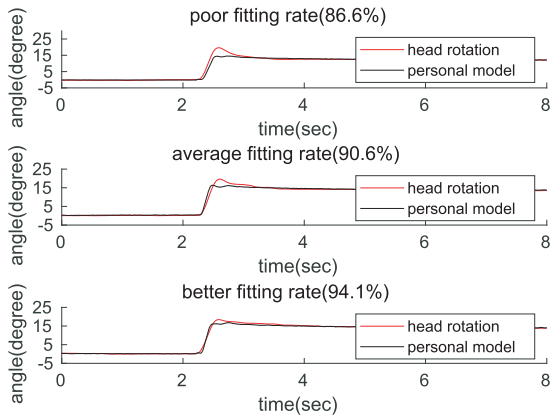

Fig. 12 Simulated outputs with personal model

Table 5 Mean of parameters for Eq. (3) (Participant A)

Parameter	mean	standard deviation
a/c	$3.54 * 10^{-1}$	0.399
b/c	2.23	1.59
d	$8.18 * 10^{-3}$	$5.97 * 10^{-3}$
e	$4.12 * 10^{-1}$	$4.86 * 10^{-1}$
f	2.80	2.31

the personal model is 87.4% and the distribution is shown in Fig. 13, which is worse than the average of fitting rate for each trial. Examples of simulated output with the obtained parameters are shown in Fig. 12. The personal model cannot always estimate the peak time or overshoot, and this results in the low fitting rate.

5.4 Variations of Head Rotation

We observed a range of different behaviors for the participants as shown in Fig. 6. Here, we examine the variations in detail by considering how Eq. (4) may fit them. Figure 14 and 15 show the simulation results with different values of T_1, T_2, and τ_3 in Eq. (5). We conclude that,

- With larger T_1, the overshoot becomes smaller or disappears. This implies that rotation slowly and asymptotically reaches to the final value, when the activation of the agonist is slow and gentle.
- With large T_2, the convergent speed of the overshoots became slower. It slowly converges because activation of the antagonist is slow and gentle.
- With smaller τ_3, the amount of the overshoots decreases. This implies that when the time difference between the agonist and the antagonist activation is smaller, the amount of overshoot becomes smaller while the convergent speed is approximately constant.

Those suggest that the activation conditions of agonist and

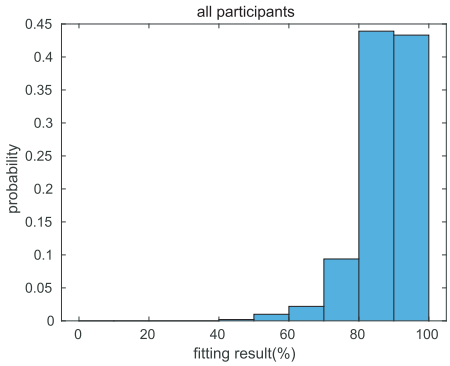

Fig. 13 Fitting rate of simulation by personal model

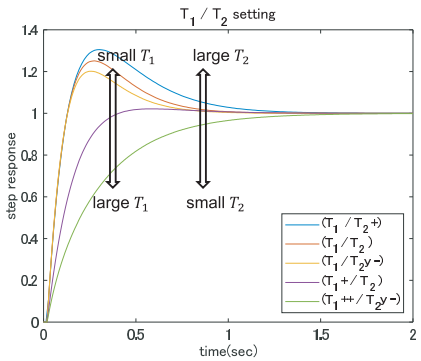

Fig. 14 Output changes with different T_1 and T_2 values (T_1+, T_2+: larger, T_1-, T_2-: smaller)

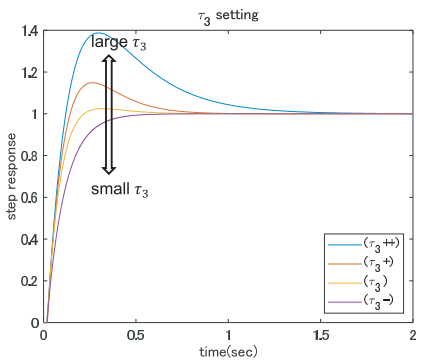

Fig. 15 Output changes with different τ_3 values ($\tau_3 + +$: largest, $\tau_3 - -$: smallest)

antagonist, i.e., the balance of T_1, T_2, and τ_3, may explain the variety of outputs as shown in Fig. 6. However, the physiological investigation is necessary to verify the above idea, which is left for future work. Dominant agonist and antagonist for head rotations are a pair of the Sternocleidomastoid muscles and their analyses would delineate the mechanism of the above model.

5.5 Discussion

The presented device gives stimulation via skin sensation. Such input to this man-machine system is affected by the installing condition of the device, the skin sensitivity, active head rotation, and perception of the head rotation.

Our experimental results show a variety of outputs with different gain and overshoots. Through examining the results, we consider the following points. First, the experiments demonstrated that participants can distinguish information through skin stretching and rotate their head with a resolution of less than 5 degrees. The experimental results also show that the characteristics of the system are relatively stable for the same person within the same installation of the device. Next, a variety of different outputs can be explained by using a relatively simple model based on kinesiology. It suggests that overshoot or settling time differences may be caused by the activation balance of the agonist and the antagonist muscles, i.e., their slow or quick activation.

The above results show that the property of the total system as a human-in-the-loop communication and guidance system can be achieved with small errors while the same installation conditions of the device hold. Consequently, the system can guide human motion provided we undertake calibration after the installation of the device.

6. Conclusion

In this paper, we introduced a novel skin-stretcher device for inducing head rotation. First, we presented the design and the mechanism of the device that utilizes the sensation of local skin displacement. Then, we reported its fundamental performance obtained through experiments.

The results show that the characteristics of the system are relatively stable for the same person within the same installation of the device, although this may change across installations and users. The transfer function analysis showed that the system behavior can be approximated well using a relatively simple model of agonist and antagonist muscles. However, the system parameters vary depending on activation property of the agonist and the antagonist, and it is rather difficult to obtain a unique transfer function that covers trials with different conditions.

Future study will target on the construction of more general or adjustable models. For future work on applications, we can consider a framework using our device as a remote communication device, in which motion, behavior, mood, or other quantities are transmitted and presented to a remote person. We can perceive head motions of a remote person by a combination of head rotation measurement of a person and stimulation to another person with the proposed device. We can expect that it provides a good channel for transmitting a remote person's states and activities. Head rotation is often caused by the intention of looking at or paying attention to a target, it suggests when and how a remote person pays attention to something. Head rotation also reflects the posture and motions of a person. Based on these characteristics, one potential application is remote monitoring for nursing care. Some head motions are important clues of a patient's moving that require attention and sufficient care, e.g., sit-to-stand, walking, falling down, trials for its recovery, etc. This would provide a new communication channel that is complementary to vision, audio, or other devices.

References

[1] H. Kawasaki, H. Kimura, S. Ito, Y. Nishimoto, H. Hayashi, and Sakaeda, "Hand rehabilitation support system based on self-motion control, with a clinical case report," 2006 World Automation Congress, pp.1–6, July 2006.
[2] M. Doi, H. Inoue, Y. Aoki, and O. Oshiro, "Video surveillance system for elderly person living alone by person tracking and fall detection," IEEJ Trans. SM., vol.126, no.8, pp.457–463, 2006.
[3] J. Rossiter, E. Knoop, and Y. Nakamura, "Affective Touch and Low Power Artificial Muscles for Rehabilitative and Assistive Wearable Soft Robotics," Wearable Robotics: Challenges and Trends, Biosystems & Biorobotics, vol.16, pp.101–106, Springer International Publishing, Cham, 2017.
[4] K. Aoyama, H. Iizuka, H. Ando, and T. Maeda, "Four-pole galvanic vestibular stimulation causes body sway about three axes," Scientific reports, vol.5, no.1, p.10168, 2015.
[5] T. Maeda, H. Ando, H. Iizuka, T. Yonemura, D. Kondo, and Y. Hashimoto, "Immersive tele-collaboration with parasitic humanoid: How to assist behavior directly in mutual telepresence," The 21st International Conference on Artificial Reality and Telexistence (ICAT 2011), Nov. 2011.
[6] T. Asakura, K. Kondo, Y. Nakamura, J. Akita, M. Toda, and S. Sakurazawa, "Sonic representation of myoelectric information: Assignments of sound features to myoelectric features and emphasis," IEICE Technical Report (Institute of Electronics, Information and Communication Engineers), vol.111, no.38, pp.73–74, May 2011.
[7] Y. Kon, T. Nakamura, and H. Kajimoto, "HangerON: A belt-type human walking controller using the hanger reflex haptic illusion," ACM SIGGRAPH 2017 Emerging Technologies, SIGGRAPH '17, pp.10:1–10:2, New York, NY, USA, 2017.
[8] T. Amemiya, "Directed force perception when holding a nonground-ing force display in the air," Proc. EuroHaptics 2006, pp.317–324, 2006.
[9] A. Ion, E.J. Wang, and P. Baudisch, "Skin drag displays: Dragging a physical tactor across the user's skin produces a stronger tactile stimulus than vibrotactile," Proc. 33rd Annual ACM Conference on Human Factors in Computing Systems, CHI '15, pp.2501–2504, New York, NY, USA, 2015.
[10] Y. Mizukami, K. Uchida, and H. Sawada, "Tactile transmission by higher-level perception using vibration of shape memory alloy thread," IPSJ Journal, vol.48, no.12, pp.3739–3749, Dec. 2007.
[11] E. Knoop and J. Rossiter, "The Tickler: A compliant wearable tactile display for stroking and tickling," Proc. 33rd Annual ACM Conference Extended Abstracts on Human Factors in Computing Systems - CHI EA '15, pp.1133–1138, 2015.
[12] V. Levesque, J. Pasquero, and V. Hayward, "Braille display by lateral skin deformation with the STReSS2 tactile transducer," Second Joint

EuroHaptics Conference and Symposium on Haptic Interfaces for Virtual Environment and Teleoperator Systems (WHC'07), pp.115–120, March 2007.
[13] D.G. Thelen, "Adjustment of muscle mechanics model parameters to simulate dynamic contractions in older adults," Journal of Biomechanical Engineering, vol.125, no.1, pp.70–77, 2003.
[14] R. Riener, J. Quintern, and G. Schmidt, "Biomechanical model of the human knee evaluated by neuromuscular stimulation," J. Biomech., vol.29, no.9, pp.1157–1167, 1996.
[15] R. Jailani, S.H. Zakaria, and M.O. Tokhi, "The development of quadriceps muscle model for paraplegic," Procedia Engineering, vol.41, pp.1553–1558, 2012.

Appendix A: MATLAB tfest

MATLAB "tfest" function estimates transfer functions with the specified number of poles, number of zeros, and IO delay. The instrument variable approach is used to initialize the values of the numerator and denominator of the output of tfest. See also: https://www.mathworks.com/help/ident/ref/tfest.html

Appendix B: Calculating the Fitting Rate

In order to evaluate the accuracy of fitting, we used "compare" function in MATLAB. It calculates fitting rate by the following formula.

$$fit = 100\left(1 - \frac{\|y - \hat{y}\|}{\|y - \text{mean}\,(y)\|}\right)$$

where y is the estimated value and $\hat{y}$ is the actual value.

Appendix C: Threshold for Settling Time

In order to verify the threshold for settling time, we calculated the settling time with another threshold, ±20% of the convergence value, and we compared them with the case of ±10%. The result is shown in Fig. A· 1. Threshold of ±20% cause around 10% changes of the mean and standard deviation, which are usually smaller than the difference within the same person. With ±10% as the convergence value, the mean and standard deviation are 125% and $8.14 * 10^3$, while they are 137% and $1.16 * 10^4$ with ±20%. Considering this, we used ±10%, that is more severe, for the analyses in this paper.

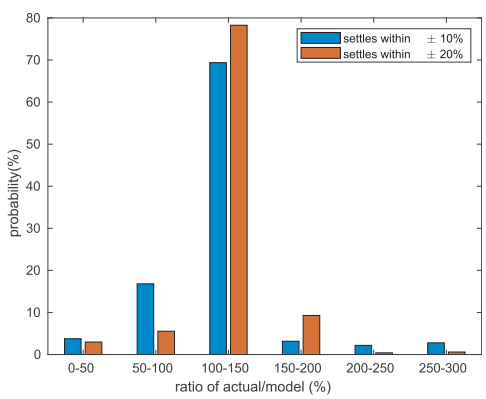

Fig. A· 1 Comparison of rules of settling time for all participants

Takahide Ito received the B.S. degrees in Electrical and Electronic Engineering from Kyoto University in 2016. He is studying electrical engineering at the postgraduate program.

Yuichi Nakamura received B.E, M.E, and Ph.D degrees in electrical engineering from Kyoto University, in 1985, 1987, and 1992, respectively. From 1990 to 1993, he worked as an instructor at the Department of Electrical Engineering of Kyoto University. From 1993 to 2004, he worked for Institute of Information Sciences and Electronics of University of Tsukuba, Institute of Engineering Mechanics and Systems of University of Tsukuba, as an assistant professor and an associate professor, respectively. Since 2004, he has been a professor of Academic Center of Computing and Media Studies, Kyoto University. His research interests are on computer vision, multimedia, human-computer and human-human interaction including distance communication, and multimedia contents production.

Kazuaki Kondo received his M. E. and Ph. D. degrees from Osaka University in Japan. He became a research associate at Osaka University in 2007, an assistant professor at Kyoto university in 2009, and a lecturer in 2015. He was awarded the Kusumoto award in 2002. His research interests are computer vision and intelligent support on human communications. He is a member of IEICE.

Espen Knoop received his M. E. and Ph. D. degrees from the University of Bristol. He became an associate research scientist at Disney Research. His research interests include soft robotics and the physical aspects of digital fabrication.

Jonathan Rossiter is Professor of Robotics and head of the Soft Robotics group at Bristol Robotics Laboratory, Royal Academy of Engineering Chair in Emerging Technologies and EPSRC Research Fellow. His research includes soft robotics, bio-mimetics, artificial intelligence, composites, sensors, and the wider robotics field.